How Particle Shape Affect Granular Segregation in Industrial and Geophysical Flows

Fernando David Cúñez[a], Div Patel[a], and Rachel C. Glade[a,b,1]

[a]Earth and Environmental Sciences, University of Rochester, 227 Hutchison Hall, Rochester, NY 14627, USA; [b]Mechanical Engineering, University of Rochester, 235 Hopeman Building, P.O. Box 270132, Rochester, NY 14627, USA

[1]To whom correspondence should be addressed. E-mail: rachel.glade@rochester.edu

How particle shape affects granular segregation in industrial and geophysical flows

Fernando David Cúñez[a], **Div Patel**[a], **and Rachel C. Glade**[a,b,1]

[a]Earth and Environmental Sciences, University of Rochester, 227 Hutchison Hall, Rochester, NY 14627, USA; [b]Mechanical Engineering, University of Rochester, 235 Hopeman Building, P.O. Box 270132, Rochester, NY 14627, USA

This manuscript was compiled on April 28, 2023

Industrial and environmental granular flows commonly exhibit a phenomenon known as "granular segregation," in which grains separate according to physical characteristics (size, shape, density), interfering with industrial applications (cement mixing, medicine and food production) and fundamentally altering the behavior of geophysical flows (landslides, debris flows, pyroclastic flows, riverbeds). While size-induced segregation has been well studied, the role of grain shape is not well understood. Here we conduct numerical experiments to investigate how grain shape affects granular segregation due to grain-grain and grain-fluid interactions. To isolate the former, we compare dry, bidisperse mixtures of spheres alone with mixtures of spheres and cubes in a rotating drum. Results show that while segregation generally increases with particle size ratio, the presence of cubes decreases segregation levels compared to cases with only spheres. Further, we find hysteresis in segregation trends with size ratio; segregation is lowest when the small grains are cubic as they approach a jammed state with reduced mobility. We find similar hysteresis in simulations of a shear-driven coupled fluid-granular flow (e.g., a riverbed), demonstrating that this phenomenon is not unique to rotating drums; however, in contrast to the dry system, we find that total segregation increases in the presence of cubic grains, and fluid drag effects can qualitatively change segregation trends. Our findings demonstrate competing shape-induced segregation patterns in wet and dry flows—independently from grain size controls—with implications for many industrial and geophysical processes.

segregation | brazil nut effect | armoring | rivers | shape

Granular materials are commonly found in our daily lives in a multitude of industrial applications (e.g., cement, pharmaceuticals, food grains) (Figure 1a,b) and in nature (e.g., rocks, sand, snow, soil). Because these materials can behave as solids, liquids or gases under the influence of external forces, they have no single constitutive equation and we have yet to gain a complete understanding of their complex behavior (1, 2). Further, mixtures of granular materials commonly exhibit an emergent phenomenon known as "segregation" in which grains of different size, shape, density and roughness self-organize to prevent uniform mixing (3–5). One of the most common examples of granular segregation is the "brazil nut effect," which occurs when smaller grains fill in voids beneath the large grains when disturbed, causing large grains to migrate toward the surface over time (Figure 1c) (6). You have likely experienced this when eating a jar of nuts or pouring cereal into a bowl. Granular segregation can be a severe nuisance, interfering with a variety of mixing processes in the cement, food and pharmaceutical industries (3).

Granular segregation is also pervasive in nature, where sediment grain size ranges from very fine silt to massive boulders (7). Geophysical flows such as debris flows (Figure 1c) (8), landslides (9), pyroclastic flows (10), and slow-moving, lobate arctic soil patterns (11) exhibit strong segregation, in which large boulders tend to organize at the front of the flow, increasing runout distance and destructive potential (3, 12). Segregation also occurs for granular beds driven by shear flows, such as wind-blown or subaqueous ripples and dunes (13, 14), beaches (15), and riverbeds where large grains can armor the surface and influence erosion rates and sediment transport dynamics (16, 17). These processes are ubiquitous not only on Earth but on other planetary bodies, including asteroids (18) and any planet or moon with a granular surface (Figure 1d)(19–21).

While granular segregation for the simplified case of spherical grains has been extensively studied (22–24), our ability to predict and control its effect in industrial or natural settings is limited; complex interactions between size, density, frictional, shape effects and disturbance rate can lead to unexpected outcomes (3, 25). One of the least explored aspects of segregation is the role of shape, though the presence of non-spherical grains is ubiquitous in most industrial and natural flows (26). Some previous studies have examined the role of grain shape in controlling rotating drum segregation patterns, showing that the presence of angular shapes can dissipate more rotational energy, affecting how they interact with the wall and with each other (5, 26–28). Grain shape has been shown to alter mobility in a variety of flow regimes, with sharp edges of cubes dissipating energy faster than spheres and decreasing mobility (28–30). However, findings from these studies are often seemingly conflicting and have been difficult to synthesize because

Significance Statement

Granular materials like cereal, pharmaceuticals, sand and concrete commonly organize such that grains segregate according to size rather than uniformly mixing. For example, in a jar of nuts, the largest ones are commonly found at the top. Here, we use computer simulations to explore how grain shape controls this phenomenon in industrial and natural settings. We find that even small differences in shape can substantially change the amount and style of segregation, with different effects depending on whether the system is wet or dry. This study demonstrates the importance of grain shape in different systems ranging from food and medicine production to geophysical hazards and processes such as landslides, river erosion, and debris flows on Earth and other celestial bodies.

F.D.C. performed research; F.D.C. and R.C.G. designed research; F.D.C, D.P. and R.C.G. analyzed data, and wrote the paper.

The authors declare no competing interest.

[1]To whom correspondence should be addressed. E-mail: rachel.glade@rochester.edu

Fig. 1. Processes of granular segregation. (a) Brazil nut effect in a jar of nuts. (b) Process of mixing cement. Inset: Granular mixture in a rotary drum composed by marbles with diameters of $d_s = 4$ and $d_b = 8$mm. (c) Granular segregation in the front of the Illgraben debris flow. Photo by Pierre Zufferey. Image credit: American Geophysical Union. (d) Debris flow deposit-terminations in Kepler moon crater (latitude 8.32^{o}N, longitude 37.69^{o}W)(20). (1) Finer-grained fractions (fines), (2) coarse dark levees, and (3) terminal deposits.

it is nontrivial to disentangle the role of shape and size, and different filling levels and rotational speeds used in different studies can result in complex, unpredictable radial segregation patterns that are challenging to compare (4, 29–34). Only recently has a universal rule been proposed for segregation with different shapes; (5, 26) found that segregation levels for bidisperse grains (disks, rods, spheres) in a numerical model depends largely on the volume ratio between the two species. According to their results, segregation intensity increases logarithmically with volume ratio, and grains with equal volume exhibit zero segregation. This promising work demonstrates that differences in grain volume can account for shape effects on segregation; however, their results show that segregation levels can still vary substantially for different shapes even within the same volume ratio. Many other questions remain, including the effect of angular shapes, shapes that exhibit negative curvature, and the presence of a fluid.

Here we use numerical models building in complexity to explore the role of grain shape in controlling granular segregation. First, we examine a partially-filled rotating drum filled with dry, bidisperse grains (spheres and cubes) at a low rotational velocity. We choose this setup because it is relevant not only for industrial mixing applications, but also for geophysical flows such as debris flows and landslides. We choose to compare spheres with cubes because they are not too dissimilar in shape; thus our findings may demonstrate how even mild shape differences control segregation, leaving more extreme shapes (long rods, stars, etc.) to future studies. We explicitly control for grain size by comparing results for bidisperse spheres alone with results for bidisperse mixtures of spheres and cubes and find that the presence of cubic grains not only changes segregation levels, but leads to hysteresis in segregation as small cubic grains approaching a jammed state. Next, we test numerically whether this finding applies in an entirely different system in which fluid shear drives motion over a granular bed (e.g., a riverbed). While we find similar hysteresis, results show that the presence of fluid drag can qualitatively alter segregation trends, resulting in 1) larger segregation levels in runs with cubic grains for all cases and 2) inverse segregation in which smaller cubes organize at the bed surface. Our work shows that grain shape can exert a fundamental control on segregation, both quantitatively and qualitatively, in industrial and geophysical flows. These findings demonstrate the need for more attention on grain shape to understand granular dynamics, with implications for efforts to control granular segregation in industry, predict the behavior of destructive geophysical flows, and understand sediment dynamics in rivers and windblown dunes that are pervasive on Earth and other planets.

Grain shape controls on segregation in a dry rotating drum

To isolate the purely granular effects of shape while controlling for size differences, we run dry, bidisperse models in a rotating drum with varying volume ratio for cases with 1) only spheres or only cubes with varying volume ratio ($1.3 \leq V_l/V_s \leq 30$), where V_l and V_s are the volumes of each particle for the large and small species, respectively; 2) mixtures of spheres and cubes varying the volume ratio ($0.03 \leq V_\square/V_\circ \leq 30$), where $V_\square$ and $V_\circ$ are the volumes of each particle for the cubical and spherical species, respectively. By examining differences in segregation between these cases for the same volume ratios, we can truly isolate the effects of shape.

We use the open-source code LIGGGHTS, which is based on the Discrete Element Method (DEM), to compute granular dynamics. While LIGGGHTS was originally designed to simulate spherical grains, we take advantage of two recently developed capabilities to simulate cubic grains: bonded spheres (Figure 2a) and superquadrics (Figure 2b). Superquadrics allow simulations of near-realistic shapes such as rods, ellipsoids and more angular shapes such as cubes (albeit with slightly rounded edges). However, state of the art coupled fluid-granular models are not yet able to simulated superquadrics because fluid drag formulations only work for groups of spherical grains (35, 36). Therefore, we also use bonded spheres to create lumpy cubic grains of various sizes (hereafter referred to as "bonded cubes") in order to test whether this approach can be a good approximation for real shapes in fluid simulations. These bonded cubes also allow us to explore effects of grain shapes with negative curvature (Figure 2a) (37). We calculate the total volume of the bonded cubes as the total volume of the bonded spheres, plus the volume of the void space in the middle of the grain. We slightly increase the density of each bonded spheres to account for this void space, allowing for equal effective density of bonded cubic grains and other grains (see Methods). Cubes and spheres are initially randomly distributed within the drum at equal volumes between the two species, with a packing fraction of around 30%, and the drum is driven at a low rotational speed representative of a variety of industrial and natural flows. For all cases, we calculate the final amount of segregation once the system has reached a quasi-steady state (Figure 2c) and the time that the mixtures take to reach it (See Methods). Segregation is calculated such that S=0 represented a completely mixed system (equal proportions of both grains), and S=1 represents a completely segregated system (only a single type of grain present) (see Methods). We validated segregation calculations by computing the amount of segregation in a simulation where both species were equal sized spheres, finding that the amount of segregation through time was zero (Supplemental Material). We also validated the model setup by comparing results with a physical experiment in a rotating drum, using the same rotation rate and marbles of the same size (Figure 1b; Supplemental Material).

Our results illuminate the importance of both grain size and shape in controlling segregation, clearly demonstrating that shape alone can substantially affect segregation levels. We observe similar qualitative behavior for all runs; Figure 2c

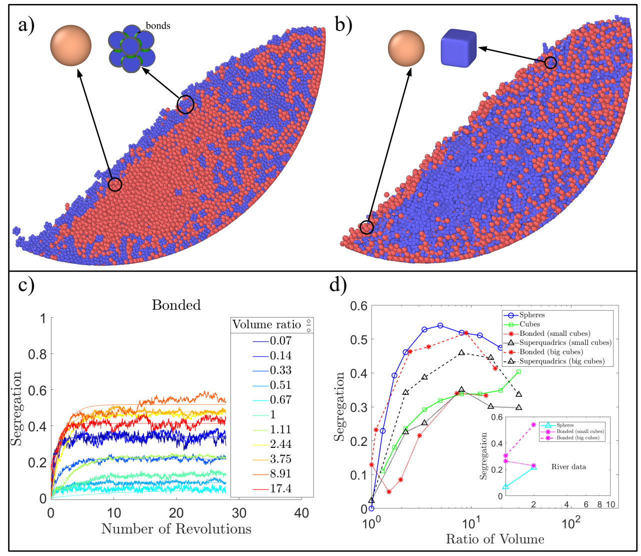

Fig. 2. (a) Snapshot of particle positions of a mixture of spheres and cubic grains developed by bonded spheres ($V_\square/V_\circ = 3.75$). (b) Snapshot of particle positions of a mixture of spheres and cubic grains developed by superquadrics ($V_\square/V_\circ = 0.45$). (c) Temporal evolution of the amount of segregation for mixtures of spheres and cubic grains (bonded spheres). (d) Final amount of segregation as a function of the ratio of volume for rotary drum cases. Inset: Final amount of segregation for fluid-sheared granular beds.

shows the evolution of the amount of segregation for mixtures of spheres and bonded particles, where cooler colors represent to small volume ratios and warmer colors to large volume ratios. In all cases the amount of segregation starts at zero, where the particles are randomly distributed and then increases until it reaches a final steady state (see Supplemental Materials for other time series). In agreement with previous studies (5, 26, 38), final segregation for all cases tends to increase with volume ratio for ratios up to about 12 (Figure 2c,d). Large grains, regardless of shape, tend to migrate toward the surface and walls of the drum as the brazil nut effect. However, once volume ratios are large enough, it is not possible to define well segregated regions in the mixture. This is due to the onset of a segregation inversion in which large grains begin to accumulate at the center of the drum (Supplemental Materials). This result agrees with previous studies that found inverse segregation for large size ratios, where depending on the roughness of the walls and the weight of the grains, large grains may condensate in the center of the drum (30, 39, 40).

The effect of grain shape lies in substantial quantitative differences in segregation levels in all runs. The presence of cubic grains decreases segregation in most cases, except for the case of equal volume in which non-spherical grains produce slightly higher segregation levels, in contrast to previous findings (5, 26) (Figure 2d). Runs with superquadric cubes alone exhibit nearly half the segregation levels as spheres alone. However, the most surprising result is found for mixtures of cubes and spheres. We observe a hysteresis in segregation trends, where segregation levels are lowest for cases in which cubes are smaller than spheres, and higher for cases in which cubes are larger than spheres for the same volume ratio; this occurs for both superquadric and bonded cubes (Figure 2d). Superquadrics exhibit lower segregation than comparable bonded cube cases; while runs with large bonded cubes and small spheres are nearly identical runs with spheres alone, runs with larger superquadric cubes experience less segregation. The lowest values of segregation occur for cases with small superquadric or bonded cubes mixed with spheres.

Anisotropy and the approach to shear jamming

Our results demonstrate clear shape controls on granular segregation and previously unobserved hysteresis in segregation depending on grain shape. The shape of the smaller grains controls granular segregation behavior in the drum, with possible implications for industrial applications where segregation is unwanted and our ability to understand and predict segregation processes in granular flows. But how can we explain the observed hysteresis and importance of the shape of small grains?

To better understand our results, we analyze snapshots of model runs at steady state segregation and dive into the small scale interactions between individual grains. By examining grain dynamics in zoomed in videos of model runs (Supplemental Materials), we observe that cubic grains tend to align along their edges and inhibit mobility in the center of the drum. We hypothesize that this behavior can be associated with an approach to a shear jamming state, in which grains experience an increase in the number of contact points with other grains as well as anisotropy related to the direction of the applied stress, thus leading to structure between grains and reduced mobility (41). While jamming behavior is not often associated with granular segregation dynamics in the literature, it is intuitive that they should be related; if granular segregation depends largely on percolation of small grains through a network of larger grains, then the mobility of the small grains depending on shape and size must matter. While most jamming has been observed in monodisperse systems, it has recently been observed in bidisperse mixtures (42); further, because segregation tends to separate grains based on physical characteristics, through time grains tend to interact with other grains of the same size and shape. Previous studies of hopper flow have observed unexplained slowing of segregation when a critical concentration of small grains is reached, likely due to the onset of jamming (43, 44). Though the continuous fluid-like motions of grains in the rotating drum prevent a fully jammed state, we propose that decreases in grain mobility may be explained by an approach to this state.

In order to test this, we examine snapshots of the model at final segregation levels to see if they exhibit certain characteristics that are hallmarks of the approach to a shear jammed state: organized force chains, anisotropy, and an increase in the number of contact points (Figure 3) (41, 45). Figure 3a shows a voronoi tesselation of a model run with superquadric cubes ($V_\square/V_\circ = 0.45$), illustrating that cubes in the center of the drum tend to be tightly packed with minimal void space between neighbors. This is due to the preferential alignment of the cubes with the direction of shear making the orientation of the cubes uniform and letting them align face to face. A more random orientation of cubes would increase the effective space any individual cube takes up, preventing the cubes from packing together as densely. Figure 3b shows a snapshot of the magnitude of force chains throughout the drum; long force chains are strongly aligned in the direction of shear, with strong connections between cubic grains in the center of the drum. This differs from cases in which cubes are larger than spheres, where force chains are shorter and more randomly oriented (Supplemental Material). The alignment of force chains suggests anisotropy, another common hallmark of the approach to jamming, in which grains are preferentially aligned and therefore exhibit greater structure (and lower mobility) than randomly oriented grains (41, 46, 47). Fabric anisotropy refers to properties such as shear strength and dilatancy taking on different values along different directions due to the state of the granular material's microstructure, where microstructure refers to the arrangement of particles, void spaces, and interparticle contacts (48). Though it could be characterised with the arrangement of particles and void spaces, this study characterises the microstructure with a fabric tensor based on inter-particle contacts due to forces being transmitted along these contacts, forming force chains (see Methods for the mathematical formulation of the fabric tensor). Granular mixtures with fabric anisotropy may exhibit jamming along directions with enhanced shear strength and thus diminished mobility in those directions. We calculate fabric anisotropy for all model runs (49) (see Methods) and find that runs with small cubic grains exhibit higher anisotropy than the equivalent runs with large cubic grains (Figure 3c). All cases with cubes exhibit higher anisotropy than for spheres alone, and superquadric cubes exhibit higher anisotropy than bonded cubes. This can be explained due to the negative curvature of bonded cubes, such that they can fit together in a variety of ways, whereas superquadrics preferentially align face to face. The mean contact number for all cubic runs is also substantially higher than that of spherical runs (Figure 3c, inset). The mean contact number is higher for all cases involving cubes than for spheres; again, cases with small cubes experience a higher contact number than for large cubes, and superquadrics experience higher contact numbers than bonded cubes. This

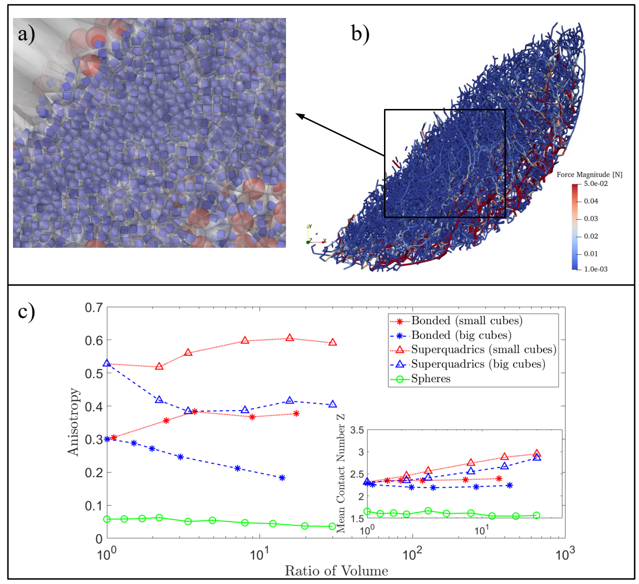

Fig. 3. (a) Zoom in of an instantaneous snapshot of particle positions of a mixture of spheres and cubic grains developed by superquadrics ($V_\square/V_\circ = 0.45$) and its voronoi tesselation. (b) Network of force chains for the same case ($V_\square/V_\circ = 0.45$). (c) Anisotropy as a function of the ratio of volume. Inset: Mean contact number per particle Z as a function of the ratio of volume.

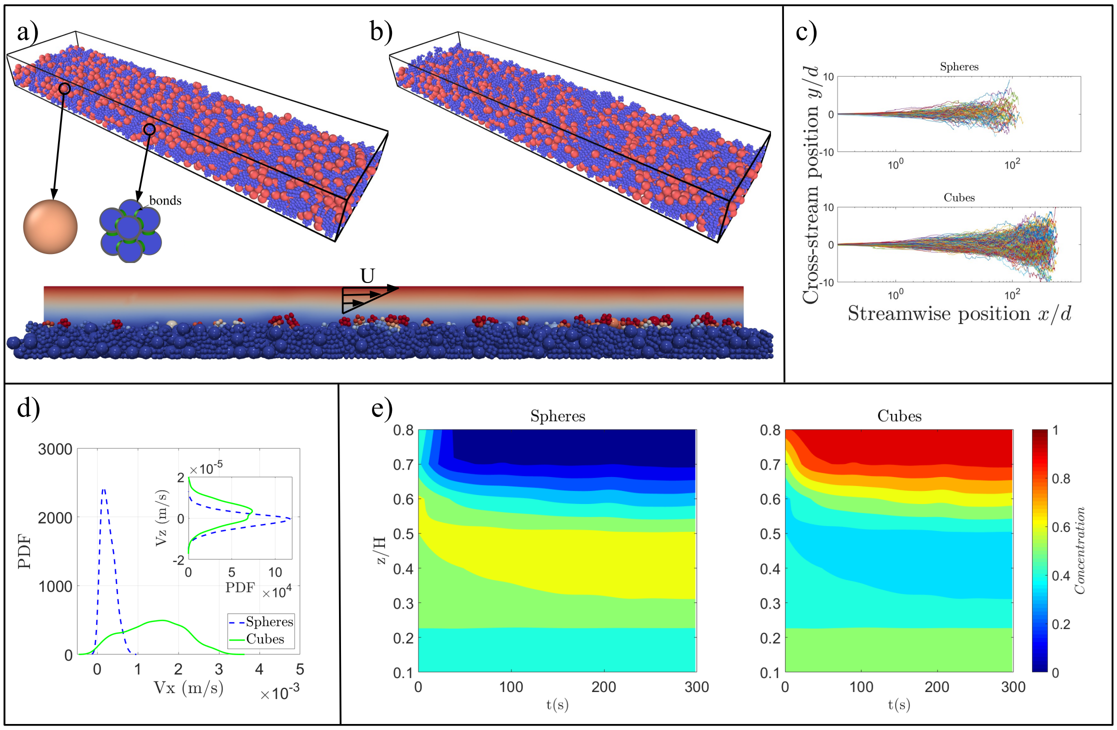

Fig. 4. River data. Snapshots of particle positions of a mixture of spheres and cubic grains developed by bonded spheres ($V_{\square}/V_{\circ} = 0.5$) at: (a) Initial condition ($t = 0s$), and (b) final state ($t = 300s$). (c) Particle trajectories. (d) Probability Density Functions (PDF) of downstream velocities and vertical velocities (inset) for each species of particles. (e) Temporal evolution of concentration of spheres and cubic grains as a function of the channel height.

analysis suggests that the presence of small cubes leads to an approach to shear jamming, causing cubes to align and experience reduced mobility in the center of the drum. This leads to a decrease in their ability to percolate, and therefore a decrease in segregation.

These findings demonstrate a new mechanism by which shape can control granular segregation levels, illustrating a previously unexplored link between shear jamming and segregation efficiency. Further, the hysteresis we have identified in segregation levels demonstrates the importance of the small size fraction in controlling segregation. This aligns with the prevailing hypothesis that the brazil nut effect is generally controlled by percolation of small grains; thus we anticipate that the shape of the smallest size fraction may be the dominant factor for shape-controlled segregation.

Our results also show that superquadric and bonded cubes exhibit similar segregation behaviors. In the next section we use bonded cubes in a coupled fluid-granular simulation to show that shape-induced hysteresis in segregation also occurs in an entirely different system: shear flow over a granular bed (e.g., a riverbed).

Grain shape controls on a fluid-sheared granular bed

Fluid shear flow over granular beds sculpts planetary landscapes, as wind creates ripples and dunes and rivers transport sediment, carving mountain ranges and delivering nutrients to the ocean. Granular segregation is ubiquitous in these types of flows, especially in rivers or on beaches where large grains commonly armor the bed surface. This armoring can change the morphology and dynamics of the flow, with implications for flooding, erosion and landscape evolution processes (15, 16). It is thought to occur due to a variety of processes, including preferential removal of fine grains due to sediment supply limitations (50) and granular segregation via the brazil nut effect as grains are disturbed by fluid near the surface of the bed (51, 52) and experience creep at slower rates deeper into the bed (17). However, most formulations of bedload transport in rivers assume spherical grains that do not represent natural sediment. Only recently has grain shape been shown to affect fluvial sediment transport via changes in fluid drag (53, 54) and interactions with the granular bed (53, 55). The role of grain shape in controlling granular segregation processes in natural fluid flows has been unexplored.

To begin to explore grain shape effects on segregation in natural systems, we run simulations of a Couette flow over a granular bed with bidisperse spheres and bonded cubes (Figure 4a), tracking segregation of the bed and grain velocities through time. We use the Coupled Fluid Dynamics/Discrete Element Method (CFDEM) modeling software, which couples the LIGGGHTS granular dynamics and OpenFOAM fluid dynamics models (56), to observe laminar flow over a granular bed in a rectangular channel with periodic boundary conditions in the streamwise direction. The flow velocity is set to be just above the threshold of motion ($\theta/\theta_{cr} \approx 1.5$) for the largest grains in the channel (see Methods). We choose to use laminar flow for simplicity, in order to focus on first order interactions between fluid and grains; while future studies may examine the role of turbulence characteristic in many natural flows, studies have shown that sediment transport in laminar flows is fundamentally similar to that of turbulent flows (57).

Our results show that granular segregation driven by fluid shear exhibits hysteresis similar to that seen in the dry rotating drum (Figure 2d inset), suggesting that our findings are not unique to that system. Runs with small cubes and large spheres experience only a third of the segregation level seen for runs with large cubes and small spheres. However, we find that the effects of fluid-grain interactions can lead to both quantitative and qualitative differences in segregation trends. In contrast to the rotating drum case, the presence of bonded cubes leads to higher segregation levels than spheres alone (Figure 2d inset); further, bonded cubes always organize at the top of the bed, even when they are smaller than the spheres. This can be seen for the case shown in Figure 4, in which $V_{\square}/V_{\circ} = 0.5$. Beginning from a fully mixed state (Figure 4a), the smaller blue cubes preferentially organize at the bed surface through time (Figure 4b,e). This demonstrates a new shape-induced reverse brazil nut effect in natural flows that may offset the armoring phenomenon.

Why do we observe qualitatively different segregation trends in the presence of a fluid? By analyzing individual grain velocities and distances, we find that cubes travel further distances downstream than spheres over the course of the model (Figure 4c). PDFs of grain velocities show that cubes experience faster instantaneous downstream velocities than spheres (albeit with much larger variability)(Figure 4d) and upward directed vertical velocities, while spheres subtly tend toward downward directed vertical velocities (Figure 4d inset). We can better understand this behavior by examining the concentration of each grain shape with respect to the total number of grains in a series of layers at different depths in the bed at the end of the model run (Figure 4e). At t=0, grains are randomly mixed throughout the bed. As time progresses, they experience rapid segregation in which cubes accumulate at the bed surface (approx. where z/H = 0.7). A zone of low cube concentration grows through time with depth just beneath the surface; in contrast, spheres accumulate just beneath the bed surface in a concentrated layer that grows in depth over time.

We interpret these results to illustrate the role of the fluid in driving segregation patterns in a granular bed. Because cubes experience a higher drag force than spheres (53, 58), once they reach the surface they can move faster and are more likely to continue moving. This likely prevents them from settling back into the bed, decreasing their ability to percolate and leading to higher segregation levels, causing them to collect on the bed surface even if they are smaller than the spheres. At depth, however, grain-grain interactions dominate, causing spheres to migrate upwards and collect just beneath the surface above which fluid effects take over (see high concentrations of spheres at z/H = 0.4-0.5). These findings point toward the need for further exploration of the role of fluid effects in non-spherical granular flows and may begin to explain enigmatic observations in riverbeds, where in some situations large grains armor the surface, while in other situations finer grains are found at the top (59, 60). Further work is needed to determine whether our findings apply to natural rivers, where dense sediment of many different shapes are found in turbulent flows.

Discussion

Our findings show that grain shape cannot be ignored in granular segregation processes, even when volume effects are accounted for. Shape-induced segregation trends can vary both quantitatively and qualitatively depending on competition between grain-grain and grain-fluid effects. In dry flows, we observe hystersis in which small cubic grains can experience high anisotropy and contact numbers, approaching a shear jamming state that reduces mobility and segregation, with possible implications for industrial applications where segregation is a nuisance. While we see similar hysteresis in fluid shear-driven slows, cubic grains of any size instead increase segregation levels compared to spheres alone; fluid-grain interactions can even lead to qualitative shifts in behavior, producing a reverse brazil nut effect in which small cubes accumulate at the surface. These results illuminate competing segregation effects due to grain-grain and grain-fluid interactions, which could lead to different qualitative behavior depending on the volume fraction and inertial regime of different industrial and geophysical flows.

Our methods demonstrate a way to isolate the role of grain shape from size disparities by comparing results for the same volume ratio with different shape combinations. Future studies can use this approach to examine different shapes, mixtures with more than two grain classes, and to see whether our results hold for rotating drums with different rotation rates and filling levels. Studies can also explore whether our results can be harnessed in industrial applications to decrease segregation in mixing processes by adding non-spherical grains to mixtures. While our analysis suggests that small grains are inherently important to segregation processes, further studies could explore whether it is the size or abundance of cubic grains that most strongly controls segregation; because we use an equal total volume of each species in our models, small grains are more abundant than large ones. The fact that runs with large superquadric cubes exhibit lower segregation rates than those with spheres alone illustrates that even small numbers of cubes can have an effect on segregation dynamics. It is possible that experiments with abundant large cubic grains could experience shear jamming effects similar to those we see for small cubes.

The link between the approach to shear jamming and segregation has implications not only for industry but also for geophysical flows. A recent study demonstrated that debris flow rheology is controlled by the solid volume fraction, and therefore the distance to the jamming transition (61). Another recent study found that the temporal evolution of angular grains in a pyroclastic flow determines flow rheology (62). Indeed, changes in packing fraction known to affect rheology have also been shown to result in qualitative shifts in segregation trends (63). In light of these studies and our findings, we suggest that grain shape exerts a fundamental control on both the segregation and rheology–and therefore destructive potential–of geophysical flows. While our fluid shear-driven model applies to riverbeds, beaches, and possibly windblown settings–examples of dilute suspensions where the volume of moving sediment is low compared to the volume of the fluid (2)–future work could explore whether similar competition between shape-induced grain-grain and grain-fluid controls on segregation applies in industrial and natural systems that behave as dense suspensions (64), such as cement mixers (65), debris flows and landslides (2). Further work could explore shape-induced granular segregation processes in non-inertial systems over longer timescales, such as hillslopes that evolve through slow soil creep or crystal segregation in magmas (66).

Materials and Methods

Model Description. In our numerical simulations for the purely granular effects, we used the open source code LIGGGHTS (67, 68) and its modified version that includes bond equations (35) to compute the interactions of each individual particle and the wall by solving the linear and angular momentum equations, given by Eqs. 1 and 2, respectively:

$$m\frac{d\vec{u}}{dt} = \sum_{i\neq j}^{N_c} \vec{F}_{c,ij} + \sum_{i}^{N_w} \vec{F}_{c,iw} + m\vec{g} \quad [1]$$

$$I\frac{d\vec{\omega}}{dt} = \sum_{i\neq j}^{N_c} \vec{T}_{c,ij} + \sum_{i}^{N_w} \vec{T}_{c,iw} \quad [2]$$

where $\vec{g}$ is the acceleration of gravity and, for each solid particle, m is the mass, $\vec{u}$ the velocity, I the moment of inertia, $\vec{\omega}$ the angular velocity, $\vec{F_c}$ the resultant of contact forces, and $\vec{T}$ the resultant of contact torques. The indices in F_c and T correspond to the collisions between particles i and j, and between particle i and the wall w.

To compute the contact forces between particles $\vec{F}_{c,ij}$ and between particles and the rotational wall $\vec{F}_{c,iw}$, we use the Hertzian contact theory (69) which consists of a system with two springs to represent the normal and tangential forces acting between two spheres colliding. The DEM parameters used in this work are taken from previous studies (17, 36) and are detailed in Tab. 1.

Table 1. DEM Simulation parameters.

Particle density ρ (kg/m^3)	1190
Young's Modulus E (MPa)	5
Poisson Ratio σ	0.45
Particle-particle friction coefficientμ_p	0.5
Particle-wall friction coefficientμ_w	0.5
Coefficient of restitution ϵ	0.5
Time step ΔT (s)	1×10^{-6}
Angular velocity of the drum Ω (rpm)	12

For the fluid-sheared granular bed, the computations were carried out by using the open-source code CFDEM (56), that couples LIGGGHTS (described previously) and OpenFOAM (which computes the fluid motion in an Eulerian frame). For this case, the LIGGGHTS code solves a modified Eq. 1, where we add the fluid contributions given by $\vec{F}_D + \vec{F}_{stress} + \vec{F}_{am}$ in the right-hand side, where $\vec{F}_D$ is the drag force caused by the fluid on particles, $\vec{F}_{stress} = V_p[-\nabla P + \nabla \cdot \bar{\bar{\tau}}]$ is the force caused by the fluid stresses, and $\vec{F}_{am}$ is the added mass force which is important for simulations involving liquids (36). P is the fluid pressure and $\bar{\bar{\tau}}$ is the deviatoric stress tensor of the fluid. On the other hand, OpenFoam computes the conservation of mass and momentum of the fluid by the following equations:

$$\frac{\partial \rho_f \varepsilon_f}{dt} + \nabla \cdot \left(\rho_f \varepsilon_f \vec{u}_f\right) = 0 \quad [3]$$

$$\frac{\partial \rho_f \varepsilon_f \vec{u}_f}{dt} + \nabla \cdot \left(\rho_f \varepsilon_f \vec{u}_f \vec{u}_f\right) = -\varepsilon_f \nabla P + \varepsilon_f \nabla \cdot \bar{\bar{\tau}} - \frac{\vec{F}_D}{V_{cell}} \quad [4]$$

where $\vec{u}_f$ is the velocity of the fluid phase, ε is the volume fraction of the fluid in a calculation cell, and V_{cell} is the volume of the considered calculation cell. The estimations of the drag force $\vec{F}_D$ imposed on each particle come from experimental correlations based in the flow regime and the volume fraction (70). The CFD parameters used in this work are detailed in Tab. 2.

Table 2. CFD Simulation parameters.

Fluid density ρ_f (kg/m^3)	1050
Fluid viscosity μ_f (mPa.s)	72.2
Top mean velocity U (m/s)	0.02
Mean fluid height h_f (m)	0.004
Time step ΔT_f (s)	5×10^{-5}
Channel dimensions X, Y, Z (m)	$0.1 \times 0.025 \times 0.01$

With the conditions described above, the Reynolds number $Re_f = \rho_f U h_f / \mu_f$ is around 1.5 that assures the flow is in a laminar regime. The shields number $\theta = \frac{\mu_f U / h_f}{(\rho_p - \rho_f) g d_p}$ has values ranging from 0.13 to 0.18 (depending on the size of particles), and the threshold of motion for this case is $\theta_{cr} \approx 0.1$ (52, 71).

Numerical setup and validation. For the particles, we used: (i) Spheres with sizes varying from 1.5mm to 4.5mm. (ii) Cubical particles formed from bonded spheres, that were implemented numerically by placing into permanent contact 8 spheres, that do not overlap with each other, with bonds half the diameter of spheres and being considered solid, as shown in Fig. 2(a); in order to prevent any gravitational stratification, we match the mass of the 8 bonded spheres to the solid spheres to estimate the density of individual grains that composed a bonded cube. (iii) Cubical particles formed from superquadric shapes (Fig. 2(b)) which are determined by the following equation:

$$\left(\left|\frac{x}{a}\right|^{n_2} + \left|\frac{y}{b}\right|^{n_2}\right)^{\frac{n_1}{n_2}} + \left|\frac{z}{c}\right|^{n_1} - 1 = 0 \quad [5]$$

where a, b, c are the lengths of the particles semi-axis, and n_1 and n_2 determine the particle shape and the surface blockiness (5, 26, 72). To obtain the cubical particle shown in Fig. 2(b), we set n_1 and n_2 equal to 8.

For the case of the purely granular interactions, we consider a rotary drum with a diameter D of 0.3m and a width W of 0.05m driven by a rotational speed of 12RPM for 140s; meanwhile, for the case of the fluid-sheared granular bed, we used a rectangular channel with dimensions of 0.1m in the streamwise direction, 0.025m in the cross-stream direction, and 0.01m in depth; where we imposed a velocity at the top wall of 0.02m/s for 300s. For both cases, two species of particles were randomly placed in equal ratios. In order to run the numerical simulations, first we let the mixture of particles to settle for 1 second and to rest for another 1s.

As part of the validation of our dry model, we also carried out an experiment with a rotary drum filled with glass beads of various sizes (see Supplemental Material (73) for a video comparing the experiments and numerical simulations).

Calculation of the amount of segregation. Figure 2c shows the evolution of the amount of segregation for mixtures of spheres and bonded particles, where cooler colors represent to small volume ratios and warmer colors to large volume ratios. In all cases the amount of segregation starts at zero, where the particles are randomly distributed and then increases until it reaches a final steady state. For each case, we fitted the curves of the temporal evolution of the amount of segregation by using the following expression:

$$S(t) = S_f\left(1 - e^{-t/t_s}\right). \quad [6]$$

where S_f is the amount of segregation at the steady state, t is time, and t_s is the time that a case takes to reach the steady state from its initial condition.

By fitting the curves shown in Fig. 2 (c), the final amount and the time of segregation for each case were determined.

The amount of segregation that a system reaches is an important parameter to estimate the final behavior of a mixture of particles; however, it is an empirical parameter that varies with the local domain, number of species, and the distribution of particle size. Although there are several studies that focus on determining the amount of segregation, calculations are inherently biased depending on the choice of window size. To quantify segregation, we calculated the fraction of each species with respect to the total number of particles throughout the entire domain, based on dividing the rotary drum in sub-domains as shown in Ref. (74). This formulation is useful because it can be applied to systems with any number of different species, rather than being limited to bidisperse systems. Based on an exhaustive analysis of the number of subdomains needed in the rotary drum, we found that the size of a subdomain is best determined by the sum of the sizes of each species (see Supplemental Material (73) for the study of subdomain sizes).

The domain of the drum is divided in M number of subdomains of rectangular shape to estimate the amount of segregation of Q types of species present in the mixture. For our study, we consider a distribution of equal volume ratio for the granular bed; then, the domain does not contain the same number of particles of each species. Therefore, to determine the fraction of one species with respect to the highest number of particles relative to the other species is given by the following equation:

$$P_{ki} = \frac{n_{ki} f_k}{max\left(\left(n_{1i} f_1\right), \left(n_{2i} f_2\right), ..., \left(n_{Qi} f_Q\right)\right)} \leq 1. \quad [7]$$

where n_{ki} is the number of particles of the k^{th} species in the subdomain i, and f_k is the factor of participation based in the total number of particles of each species given by:

$$f_k = \frac{max\left(\sum_{i=1}^{M} n_{1i}, \sum_{i=1}^{M} n_{2i}, ..., \sum_{i=1}^{M} n_{Qi}\right)}{\sum_{i=1}^{M} n_{ki}}. \quad [8]$$

The instantaneous amount of segregation S is obtained from the arithmetic mean of the individual fractions of each species of particles k in all M subdomains, and is calculated by the following equation:

$$S = 1 - \left(\frac{1}{N} \sum_{i=1}^{M} \left[\frac{1}{Q-1}\left(\sum_{k=1}^{Q} P_{ki} - 1\right) \sum_{k=1}^{Q} \left(n_{ki}\right)\right]\right). \quad [9]$$

where N is the total number of particles in the mixture.

We used the segregation time series to calculate final segregation levels for each run. We fitted the curves of the temporal evolution of the amount of segregation by using the following expression:

$$S(t) = S_f \left(1 - e^{-t/t_s}\right). \quad [10]$$

where S_f is the amount of segregation at the steady state, t is time, and t_s is the time that a case takes to reach the steady state from its initial condition. By fitting the curves shown in Figure 2c, for example, the final amount and the time of segregation for each case were determined.

A. Calculation of Anisotropy. The amount of anisotropy that a granular system exhibits is determined by the contact fabric tensor $\hat{R}$, which is calculated by the following equation:

$$\hat{R} = \frac{1}{N_c} \sum_{i \neq j} \frac{\vec{r_{ij}}}{|\vec{r_{ij}}|} \otimes \frac{\vec{r_{ij}}}{|\vec{r_{ij}}|}. \quad [11]$$

where $\vec{r_{ij}}$ is the contact vector from the center of particle i to the interparticle contact between particles i and j, $\otimes$ is the vector outer product, and N_c is the total number of particles with at least two contacts. The dimensionless fabric anisotropy tensor $\hat{AF}$ is proportional to the deviatoric part of the contact fabric tensor $\hat{R}$ and can be estimated by the following expression (49):

$$\hat{AF} = \frac{5}{2}(3\hat{R} - \hat{I}). \quad [12]$$

where $\hat{I}$ is the identity tensor. Finally, the amount of anisotropy that a system shows AF is given by the norm of the dimensionless fabric anisotropy tensor and can be computed by:

$$AF = \sqrt{\hat{AF} : \hat{AF}}. \quad [13]$$

ACKNOWLEDGMENTS. The authors are grateful to PRF DNI Grant GR531094 for the financial support provided, and for helpful conversations with Hesam Askari and Peter Miklavcic.

1. DL Henann, K Kamrin, Continuum modeling of secondary rheology in dense granular materials. *Phys. review letters* **113**, 178001 (2014).
2. DJ Jerolmack, KE Daniels, Viewing earth's surface as a soft-matter landscape. *Nat. Rev. Phys.* **1**, 716–730 (2019).
3. JMNT Gray, Particle segregation in dense granular flows. *Annu. Rev. Fluid Mech.* **50**, 407–433 (2018).
4. PB Umbanhowar, RM Lueptow, JM Ottino, Modeling segregation in granular flows. *Annu. review chemical biomolecular engineering* pp. 129–153 (2019).
5. RP Jones, JM Ottino, PB Umbanhowar, RM Lueptow, Predicting segregation of nonspherical particles. *Phys. Rev. Fluids* **6**, 054301 (2021).
6. A Rosato, KJ Strandburg, F Prinz, RH Swendsen, Why the brazil nuts are on top: Size segregation of particulate matter by shaking. *Phys. review letters* **58**, 1038 (1987).
7. CM Shobe, et al., The role of infrequently mobile boulders in modulating landscape evolution and geomorphic hazards. *Earth-Science Rev.* **220**, 103717 (2021).
8. T Takahashi, H Nakagawa, T Harada, Y Yamashiki, Routing debris flows with particle segregation. *J. Hydraul. Eng.* **118**, 1490–1507 (1992).
9. L Zhang, Y Xu, R Huang, D Chang, Particle flow and segregation in a giant landslide event triggered by the 2008 wenchuan earthquake, sichuan, china. *Nat. Hazards Earth Syst. Sci.* **11**, 1153–1162 (2011).
10. E Calder, R Sparks, M Gardeweg, Erosion, transport and segregation of pumice and lithic clasts in pyroclastic flows inferred from ignimbrite at lascar volcano, chile. *J. Volcanol. Geotherm. Res.* **104**, 201–235 (2000).
11. RC Glade, MM Fratkin, M Pouragha, A Seiphoori, JC Rowland, Arctic soil patterns analogous to fluid instabilities. *Proc. Natl. Acad. Sci.* **118**, e2101255118 (2021).
12. T De Haas, L Braat, JR Leuven, IR Lokhorst, MG Kleinhans, Effects of debris flow composition on runout, depositional mechanisms, and deposit morphology in laboratory experiments. *J. Geophys. Res. Earth Surf.* **120**, 1949–1972 (2015).
13. GM Friedman, Distinction between dune, beach, and river sands from their textural characteristics. *J. Sedimentary Res.* **31**, 514–529 (1961).
14. CA Alvarez, FD Cúñez, EM Franklin, Growth of barchan dunes of bidispersed granular mixtures. *Phys. Fluids* **33**, 051705 (2021).
15. FI Isla, Overpassing and armouring phenomena on gravel beaches. *Mar. Geol.* **110**, 369–376 (1993).
16. MF Karim, FM Holly Jr, Armoring and sorting simulation in alluvial rivers. *J. Hydraul. Eng.* **112**, 705–715 (1986).
17. B Ferdowsi, CP Ortiz, M Houssais, DJ Jerolmack, River-bed armouring as a granular segregation phenomenon. *Nat. communications* **8**, 1363 (2017).
18. S Matsumura, DC Richardson, P Michel, SR Schwartz, RL Ballouz, The brazil nut effect and its application to asteroids. *Mon. Notices Royal Astron. Soc.* **443**, 3368–3380 (2014).
19. C Güttler, I von Borstel, R Schräpler, J Blum, Granular convection and the brazil nut effect in reduced gravity. *Phys. Rev. E* **87**, 044201 (2013).
20. B Kokelaar, R Bahia, K Joy, S Viroulet, J Gray, Granular avalanches on the moon: mass-wasting conditions, processes, and features. *J. Geophys. Res. Planets* **122**, 1893–1925 (2017).
21. F Elekes, EJ Parteli, An expression for the angle of repose of dry cohesive granular materials on earth and in planetary environments. *Proc. Natl. Acad. Sci.* **118**, e2107965118 (2021).
22. F Guillard, Y Forterre, O Pouliquen, Scaling laws for segregation forces in dense sheared granular flows. *J. Fluid Mech.* **807**, R1 (2016).
23. K van der Vaart, et al., Segregation of large particles in dense granular flows suggests a granular saffman effect. *Phys. review fluids* **3**, 074303 (2018).
24. L Jing, JM Ottino, RM Lueptow, PB Umbanhowar, Rising and sinking intruders in dense granular flows. *Phys. Rev. Res.* **2**, 022069 (2020).
25. K Hill, D Khakhar, J Gilchrist, J McCarthy, J Ottino, Segregation-driven organization in chaotic granular flows. *Proc. Natl. Acad. Sci.* **96**, 11701–11706 (1999).
26. RP Jones, JM Ottino, PB Umbanhowar, RM Lueptow, Remarkable simplicity in the prediction of nonspherical particle segregation. *Phys. Rev. Res.* **2**, 042021 (2020).
27. DA Santos, MA Barrozo, CR Duarte, F Weigler, J Mellmann, Investigation of particle dynamics in a rotary drum by means of experiments and numerical simulations using dem. *Adv. Powder Technol.* **27**, 692–703 (2016).
28. GG Pereira, PW Cleary, Segregation due to particle shape of a granular mixture in a slowly rotating tumbler. *Granul. Matter* **19**, 23 (2017).
29. S He, J Gan, D Pinson, Z Zhou, Particle shape-induced radial segregation of binary mixtures in a rotating drum. *Powder technology* **341**, 157–166 (2019).
30. C Beaulieu, et al., Effect of particle angularity on flow regime transitions and segregation of bidisperse blends in a rotating drum. *Comput. Part. Mech.* **9**, 443–463 (2022).
31. X Wu, Z Zuo, S Gong, X Lu, G Xie, Numerical study of size-driven segregation of binary particles in a rotary drum with lower filling level. *Adv. Powder Technol.* **32**, 4765–4778 (2021).
32. RJ Brandao, RM Lima, RL Santos, CR Duarte, MA Barrozo, Experimental study and dem analysis of granular segregation in a rotating drum. *Powder Technol.* **364**, 1–12 (2020).
33. G Pereira, N Tran, P Cleary, Segregation of combined size and density varying binary granular mixtures in a slowly rotating tumbler. *Granul. Matter* **16**, 711–732 (2014).
34. P Chen, BJ Lochman, JM Ottino, RM Lueptow, Inversion of band patterns in spherical tumblers. *Phys. review letters* **102**, 148001 (2009).

35. M Schramm, MZ Tekeste, C Plouffe, D Harby, Estimating bond damping and bond young's modulus for a flexible wheat straw discrete element method model. *Biosyst. Eng.* **186**, 349–355 (2019).
36. FD Cúñez, NC Lima, EM Franklin, Motion and clustering of bonded particles in narrow solid–liquid fluidized beds. *Phys. Fluids* **33**, 023303 (2021).
37. L Jing, JM Ottino, RM Lueptow, PB Umbanhowar, A unified description of gravity-and kinematics-induced segregation forces in dense granular flows. *J. Fluid Mech.* **925**, A29 (2021).
38. CM Dury, GH Ristow, Competition of mixing and segregation in rotating cylinders. *Phys. fluids* **11**, 1387–1394 (1999).
39. B Yari, C Beaulieu, P Sauriol, F Bertrand, J Chaouki, Size segregation of bidisperse granular mixtures in rotating drum. *Powder Technol.* **374**, 172–184 (2020).
40. DC Hong, PV Quinn, S Luding, Reverse brazil nut problem: competition between percolation and condensation. *Phys. Rev. Lett.* **86**, 3423 (2001).
41. D Bi, J Zhang, B Chakraborty, RP Behringer, Jamming by shear. *Nature* **480**, 355–358 (2011).
42. Y Hara, H Mizuno, A Ikeda, Phase transition in the binary mixture of jammed particles with large size dispersity. *Phys. Rev. Res.* **3**, 023091 (2021).
43. P Artega, U Tüzün, Flow of binary mixtures of equal-density granules in hoppers—size segregation, flowing density and discharge rates. *Chem. engineering science* **45**, 205–223 (1990).
44. N Khola, C Wassgren, Correlations for shear-induced percolation segregation in granular shear flows. *Powder Technol.* **288**, 441–452 (2016).
45. H Vinutha, S Sastry, Disentangling the role of structure and friction in shear jamming. *Nat. Phys.* **12**, 578–583 (2016).
46. D Pan, F Meng, Y Jin, Shear hardening in frictionless amorphous solids near the jamming transition. *PNAS nexus* **2**, pgad047 (2023).
47. M Otsuki, H Hayakawa, Shear jamming, discontinuous shear thickening, and fragile states in dry granular materials under oscillatory shear. *Phys. Rev. E* **101**, 032905 (2020).
48. CF Zhao, et al., Evolution of fabric anisotropy of granular soils: X-ray tomography measurements and theoretical modelling. *Comput. Geotech.* **133**, 104046 (2021).
49. CF Zhao, NP Kruyt, An evolution law for fabric anisotropy and its application in micromechanical modelling of granular materials. *Int. journal solids structures* **196**, 53–66 (2020).
50. WE Dietrich, JW Kirchner, H Ikeda, F Iseya, Sediment supply and the development of the coarse surface layer in gravel-bedded rivers. *Nature* **340**, 215–217 (1989).
51. P Frey, M Church, How river beds move. *Science* **325**, 1509–1510 (2009).
52. FD Cúñez, EM Franklin, M Houssais, P Arratia, DJ Jerolmack, Strain hardening by sediment transport. *Phys. Rev. Res.* **4**, L022055 (2022).
53. E Deal, et al., Grain shape effects in bed load sediment transport. *Nature* **613**, 298–302 (2023).
54. M Cassel, J Lavé, A Recking, JR Malavoi, H Piégay, Bedload transport in rivers, size matters but so does shape. *Sci. Reports* **11**, 1–11 (2021).
55. SG Williams, DJ Furbish, Particle energy partitioning and transverse diffusion during rarefied travel on an experimental hillslope. *Earth Surf. Dyn.* **9**, 701–721 (2021).
56. C Goniva, C Kloss, NG Deen, JA Kuipers, S Pirker, Influence of rolling friction on single spout fluidized bed simulation. *Particuology* **10**, 582–591 (2012).
57. M Ouriemi, P Aussillous, E Guazzelli, Sediment dynamics. part 1. bed-load transport by laminar shearing flows. *J. Fluid Mech.* **636**, 295–319 (2009).
58. WE Dietrich, Settling velocity of natural particles. *Water resources research* **18**, 1615–1626 (1982).
59. G Parker, CM Toro-Escobar, Equal mobility of gravel in streams: The remains of the day. *Water Resour. Res.* **38**, 46–1 (2002).
60. TE Lisle, Particle size variations between bed load and bed material in natural gravel bed channels. *Water Resour. Res.* **31**, 1107–1118 (1995).
61. R Kostynick, et al., Rheology of debris flow materials is controlled by the distance from jamming. *Proc. Natl. Acad. Sci.* **119**, e2209109119 (2022).
62. EC Breard, et al., The fragmentation-induced fluidisation of pyroclastic density currents. *Nat. Commun.* **14**, 2079 (2023).
63. Y Fan, KM Hill, Phase transitions in shear-induced segregation of granular materials. *Phys. review letters* **106**, 218301 (2011).
64. JJ Stickel, RL Powell, Fluid mechanics and rheology of dense suspensions. *Annu. Rev. Fluid Mech.* **37**, 129–149 (2005).
65. MI Safawi, I Iwaki, T Miura, The segregation tendency in the vibration of high fluidity concrete. *Cem. concrete research* **34**, 219–226 (2004).
66. NH Sleep, Segregation of magma from a mostly crystalline mush. *Geol. Soc. Am. Bull.* **85**, 1225–1232 (1974).
67. C Kloss, CL Goniva, A new open source discrete element simulation software in *Proceedings of 5th international conference on discrete element methods.* pp. 25–26 (year?).
68. R Berger, C Kloss, A Kohlmeyer, S Pirker, Hybrid parallelization of the liggghts open-source dem code. *Powder technology* **278**, 234–247 (2015).
69. PA Cundall, OD Strack, A discrete numerical model for granular assemblies. *geotechnique* **29**, 47–65 (1979).
70. D Gidaspow, R Bezburuah, J Ding, Hydrodynamics of circulating fluidized beds: kinetic theory approach, (Illinois Inst. of Tech., Chicago, IL (United States). Dept. of Chemical), Technical report (1991).
71. M Houssais, CP Ortiz, DJ Durian, DJ Jerolmack, Onset of sediment transport is a continuous transition driven by fluid shear and granular creep. *Nat. communications* **6**, 6527 (2015).
72. S Ji, S Wang, Z Zhou, Influence of particle shape on mixing rate in rotating drums based on super-quadric dem simulations. *Adv. Powder Technol.* **31**, 3540–3550 (2020).
73. *See Suppl. Material at [URL to be inserted by publisher] for a procedure to determine correct subdomain sizes to estimate amount segregation, additional graphics force chains voronoi diagrams, movies showing comparison between a experiment a numerical simulation.* (year?).
74. M Cho, P Dutta, J Shim, A non-sampling mixing index for multicomponent mixtures. *Powder Technol.* **319**, 434–444 (2017).

Supporting Information for

How particle shape affects granular segregation in industrial and geophysical flows

Fernando David Cúñez, Div Patel, and Rachel C. Glade

Corresponding Author name.
E-mail: rachel.glade@rochester.edu

This PDF file includes:

Supporting text
Figs. S1 to S7
Legends for Movies S1 to S4

Other supporting materials for this manuscript include the following:

Movies S1 to S4

Supporting Information Text

In this document we provide additional information for key aspects of the manuscript. In section I, we show the validation of our numerical model with an experimental setup with similar dimensions. In section II, we provide some information about how we determine the window size to compute the segregation level. In section III, we show instantaneous snapshots of the particles' final state for all the cases we used to produce our dry rotating drum results. In section IV, we show instantaneous snapshots of the final state of force networks for all the cases we used to reproduce the results described in section III.

I. Validation of the numerical model. We carried out an experiment to qualitatively validate our numerical model. The experimental setup (Fig. S1i) consisted of an acrylic drum with a diameter of $D = 30$cm, a stepper motor driver which rotates the drum and is controlled by an Arduino UNO through the GRBL project (https://github.com/grbl/grbl), a set of LED lamps, and a DSLR Nikon D7500 camera. The camera and the motor driver were automatically synchronized to record and save the movies. For this specific case, we placed small marbles (d_s =4mm, yellow color in Fig. S1ii) at the bottom and then the bigger ones (d_b =8mm, red color in Fig. S1ii) just above the smaller ones. We used this initial condition in order to simulate the exact initial condition for the experiment and the numerical model; however, note that it differs from the initial condition in our main model results, which begin with a fully mixed system. This initial condition would be very difficult to implement in a physical experiment. Finally, we ran the experiment for 140s at a rotation speed of 12RPM (similar conditions to the simulations carried out for the manuscript). From Figure S1ii and movie S1, we found that the behavior of the experiment and the numerical model is highly similar in terms of segregation levels and time to reach a final segregated state.

II. Determination of the window size for segregation level calculations. We studied the influence of the size of the subdomains detailed in Figure S2 in the calculation of the amount of segregation of the system. The amount of segregation is strongly dependent on the number and the size of subdomains we have in the system. Even though many studies focused in different techniques to study either level of segregation or mixing, there is no a defined recipe to follow when picking the correct window size. For our study we divided the domain into small squared sections in the x and y directions ($\Delta = dx = dy$) throughout the width of the drum, then we varied the size of Δ from $0.25(d_s + d_b)$ (where the window is around half of the size of one species) to $10(d_s + d_b)$ (where the window is around 20 times the size of one species).

Figure S3 shows the trends of the temporal evolution of the amount of segregation for different window sizes. In the case of a very small size ($\Delta = 0.25(d_s + d_b)$), the amount of segregation is very high because we are looking at a region where only one particle can fit inside, having thus a totally segregated system in that subdomain ($S \approx 1$). For the case of a big size ($\Delta = 10(d_s + d_b)$), the region is big enough that we can encounter both species in same proportions, having thus a totally mixed system in that subdomain ($S \approx 0$). However, for the cases where size is close to the sum of both species diameters ($\Delta \approx 1(d_s + d_b)$), the behavior of the evolution of the amount of segregation is similar.

To identify which size is better to compute the amount of segregation we have two references, 1) the initial condition for all the cases is that particles are randomly distributed which S should be around zero, and 2) the amount of segregation for spheres of equal size ($d_s = d_b = 1$) is zero as the system does not have either segregation by size or shape. Therefore, the best window size to compute the level of segregation is $\Delta = 1(d_s + d_b)$, because all the cases start in the same point at t=0s (Fig S3(d)) and the results are consistent with what we see qualitatively from the particle positions snapshots (Fig S5). Finally, to get the data that are in Figure 2 of the manuscript, we shifted the curves to the zero reference that is given by the case of V_b/V_s=1.

Figure S4 shows the temporal evolution of the amount of segregation for all the tested cases and their exponential fits.

III. Final state of particles position for all the tested cases. Figure S5 shows instantaneous snapshots of particle positions for size segregation in both cases spheres and cubes.

Figure S6 shows instantaneous snapshots of particle positions for size and shape segregation in for cubes made by bonded particles and superquadrics.

IV. Final state of force networks for all the tested cases. Figure S7 shows the network of force chains for mixtures of spheres and cubical particles at t=140s of simulation.

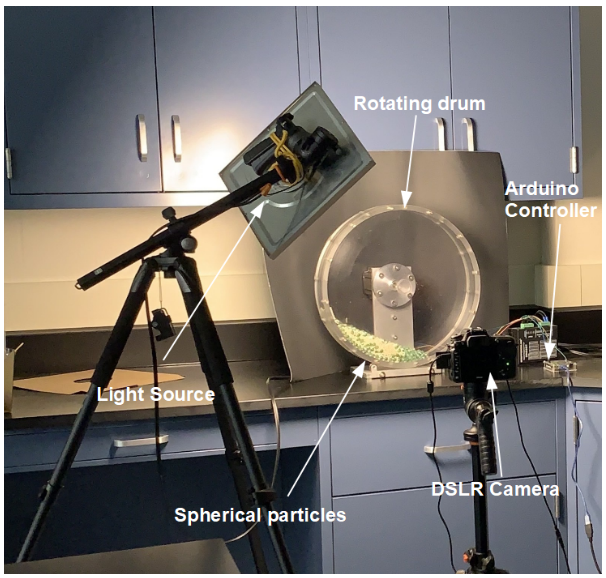

(i)

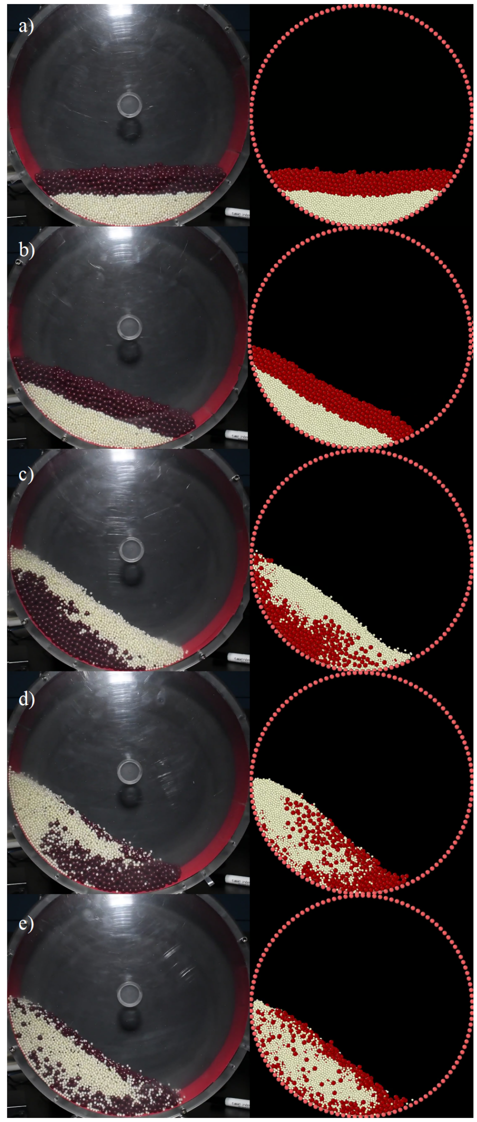

(ii)

Fig. S1. (i) Experimental setup. (ii) Comparison between the experiment (left side of the figure) and the numerical model (right hand of the figure) at: (a) t=0s, (b) t=1s, (c) t=2s, (d) t=4s, and (e) t=8s

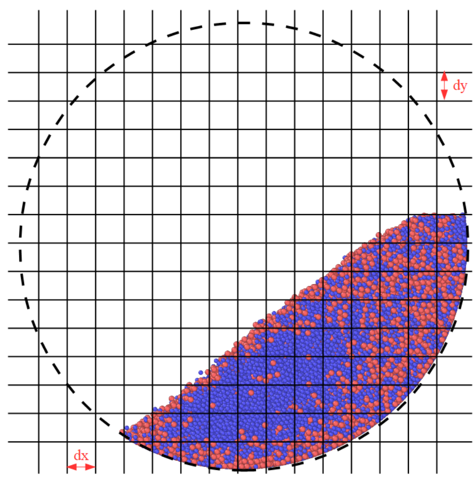

Fig. S2. Scheme of domain and subdomains considered to compute the level of segregation

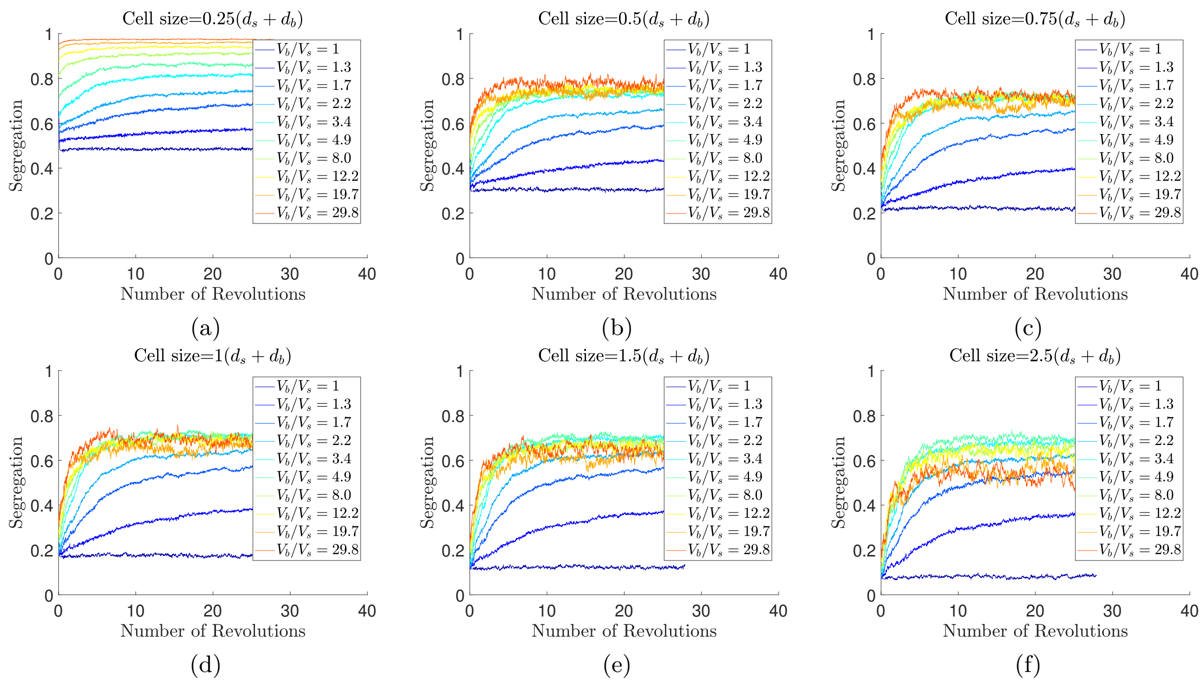

Fig. S3. Temporal evolution of the amount of segregation for mixtures containing spheres of different sizes with different window sizes. (a) 0.25$d_s + d_b$, (b) 0.5$d_s + d_b$, (c) 0.75$d_s + d_b$, (d) 1$d_s + d_b$,(e) 1.5$d_s + d_b$, and (f) 2.5$d_s + d_b$. Cooler and warmer colors show cases with small and high volume ratios, respectively.

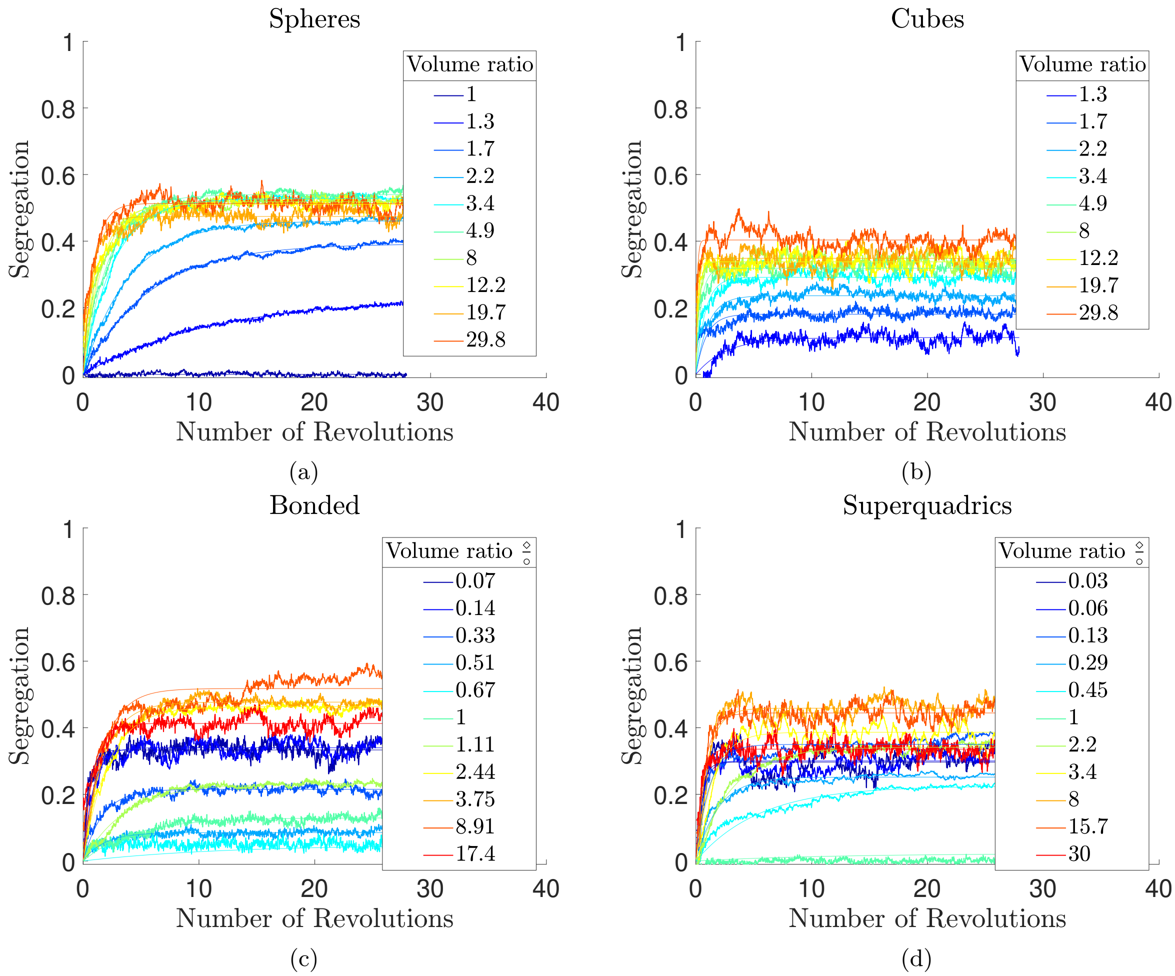

Fig. S4. Temporal evolution of the amount of segregation for mixtures containing. (a) Spheres of different sizes, (b) cubical bonded particles of different sizes, (c) spheres and cubical bonded particles, and (d) spheres and cubical superquadrics.

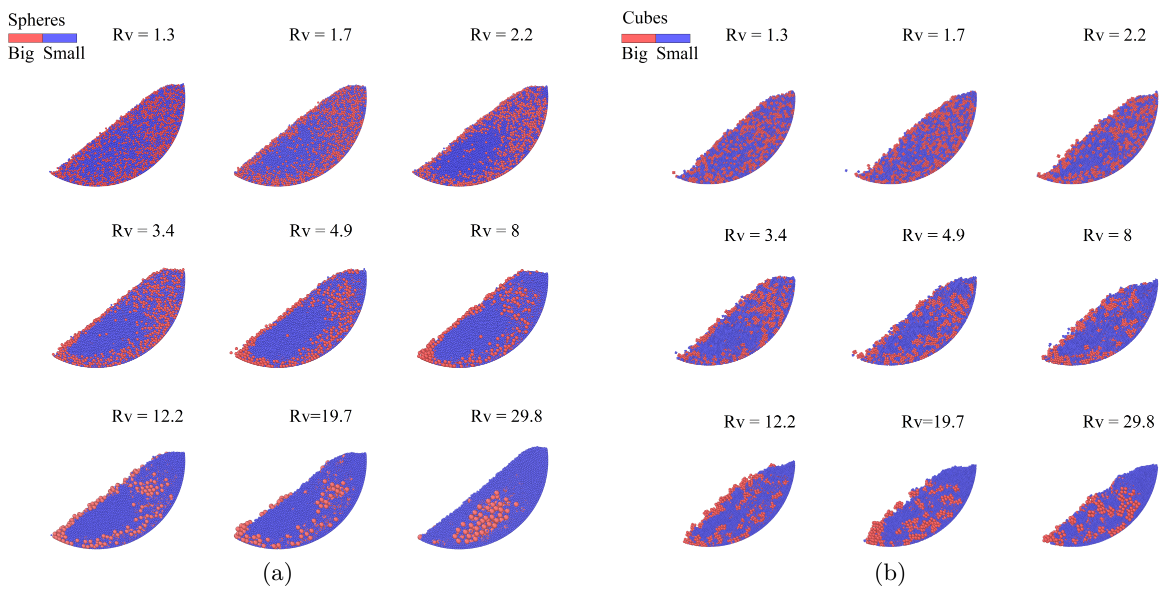

Fig. S5. Snapshots of particle positions for size segregation on: (a) spheres, (b) bonded cubes

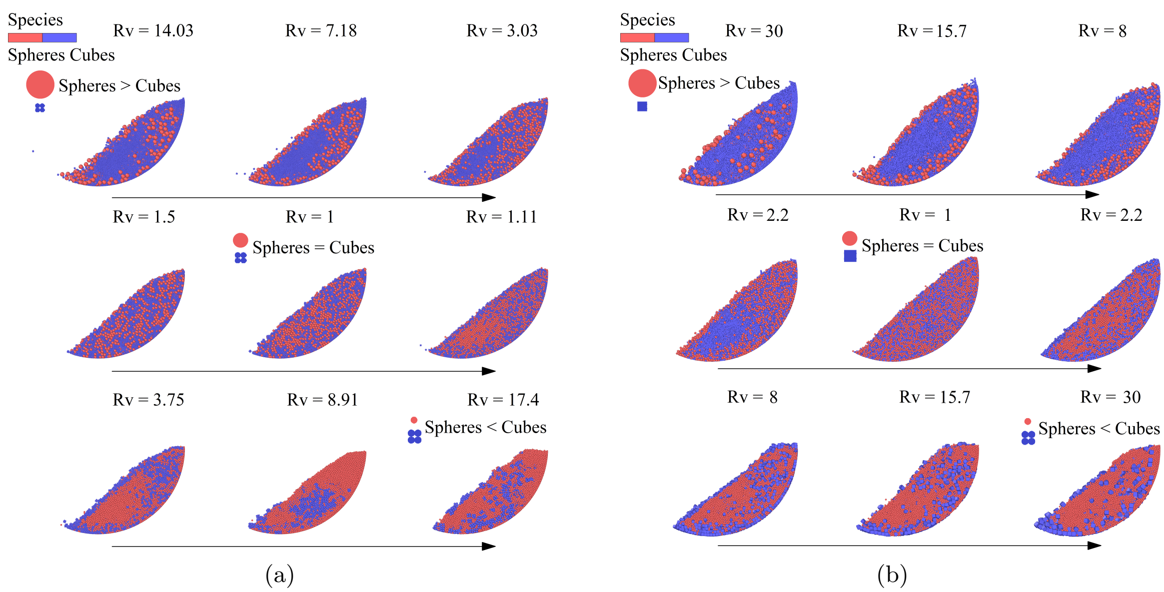

Fig. S6. Snapshots of particle positions for size and shape segregation on spheres and: (a) bonded spheres, and (b) superquadric cubes.

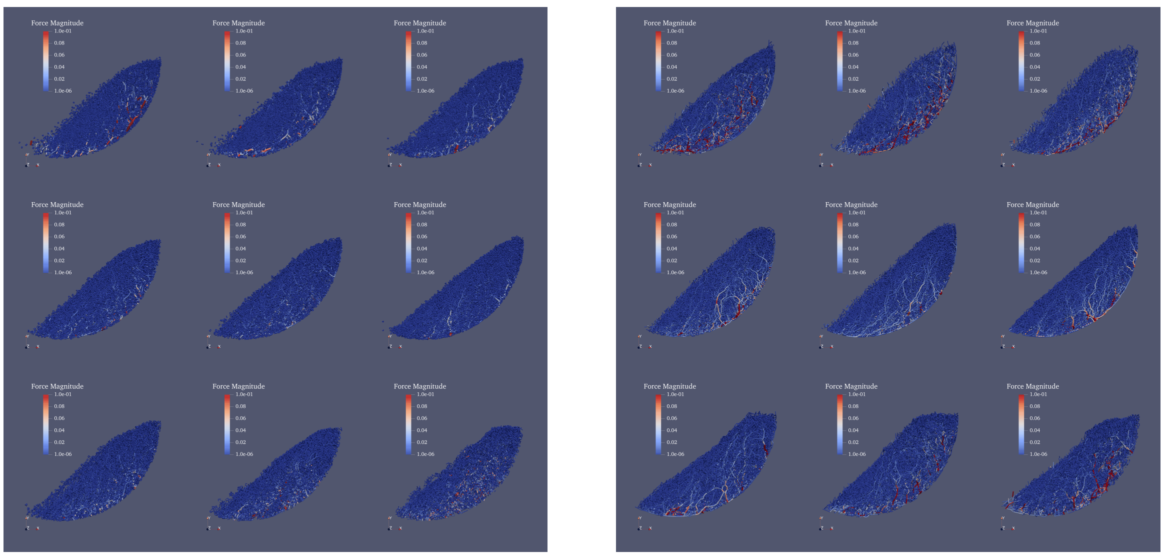

(a) (b)

Fig. S7. Snapshots of network of force chains for size and shape segregation on mixtures with spheres and: (a) bonded particles, and (b) superquadric cubes.

Movie S1. Validation of the numerical model with an experiment in real time

Movie S2. Numerical model with a mixture of spheres and bonded spheres for the case $V_{\square}/V_{\circ} = 0.07$

Movie S3. Numerical model with a mixture of spheres and cubical superquadrics for the case $V_{\square}/V_{\circ} = 0.06$

Movie S4. CFD-DEM model of a granular bed composed by spheres and bonded particles and driven by a Couette laminar flow.